Impedance Model-Based Control for an Electrohydraulic Stewart Platform

Ioannis Davliakos and Evangelos Papadopoulos*

Department of Mechanical Engineering, National Technical University of Athens, Athens 157 80, Greece

In this paper, a novel model-based impedance controller for a 6-degree-of-freedom (dof) electrohydraulic Stewart platform mechanism is developed. Rigid body and experimentally developed electrohydraulic models, including servovalve, friction and leakage models are employed and described by a set of integrated system equations. Despite the fact that an electrohydraulic servoactuator is not a source of force, as is the case with electric actuators, an impedance controller is developed for the electrohydraulic platform. This controller consists of a feedback and a model-based feedforward loop that compute servovalve currents. An impedance filter modifies the desired trajectory according to a specified behavior. This trajectory is fed to a system model in the controller aiming at a reduction of the effects of the nonlinear hydraulic dynamics. Simulations results compare system response of the developed and of a proportional-derivative (PD) controller for the electrohydraulic platform. Results during interactions with the environment show that the impedance controller is superior to available PD controllers, and that its response is smooth.

Keywords: Impedance model-based control, electro-hydraulic servosystem control, electrohydraulic interaction control.

1. Introduction

Since the original 6-degree-of-freedom (dof) Stewart–Gough platform has been developed [9, 21], and used as a flight simulator [24], a number of studies on this electrically or hydraulically driven mechanism and its variations have been published, i.e., [27]. The kinematics and dynamics of the Stewart platform have been studied by a number of researchers [7, 15, 16, 28]. However, none of these studies considered its actuation dynamics. Although electrohydraulic Stewart platforms have been used extensively, little published work on their full dynamics including actuation or their control, exists.

Impedance control is considered to be an active compliant motion control method, important in cases where force interactions with the environment occur and in industrial applications such as Computer Numerical Control (CNC), milling machines, etc. [10, 11]. Such a method is designed to offer good force accommodation and flexibility and is preferable when interactions or collisions may occur. However, impedance controllers were designed for use in systems with electromechanical actuation, since these controllers require actuators that act as force/torque sources.

Hydraulics science combined with controls, has given new thrust to hydraulics applications. The main reasons why hydraulics are preferred to electromechanical drives in a number of industrial and mobile applications, include their ability to produce large

*Correspondence to: Evangelos Papadopoulos, E-mail: egpapado
@central.ntua.gr

forces at high speeds, their high durability and stiffness, and their rapid response [14,17]. The hydraulic domain differs from the electromechanical one, in that actuator force or torque output is not proportional to input current. Therefore, hydraulic actuators cannot be modeled as force/torque sources, but rather as variable impedances. As a result, controllers that have been designed for robot control, under the assumption that actuator force/torque can be set as desired, cannot be applied in electrohydraulic systems.

A unified approach to the control of an electric manipulator applicable to free motions, kinematically constrained motions, and dynamic interaction between the manipulator and its environment has been studied in [13]. Techniques for implementing a desired manipulator impedance and for choosing the impedance appropriate to a given application using optimization theory were presented, [13]. Two spatio-geometric methods for controlling the mechanical impedance for a class of electromechanically driven Gough–Stewart platforms were presented and their response simulated in [6]. The first was based on global potential energy functions, while the second used the exponential map to associate finite displacements of the platform from equilibrium with twist displacements.

Control techniques can be used to compensate for the nonlinearities of *electrohydraulic* servosystems. Researchers have proposed nonlinear adaptive motion control techniques for hydraulic servosystems assuming linearization, [8], and backstepping, [23], approaches. A robust force controller design based on the nonlinear Quantitative Feedback Theory, has been implemented on an industrial hydraulic actuator, taking into account system and environmental uncertainties, [18].

A simulated model-based impedance control of a 3-dof redundant hydraulic parallel manipulator is presented in [22]. Further, a position-based impedance controller for an industrial hydraulic manipulator has been developed in [11]. In these works, the model is incomplete since it does not include the hydraulic dynamics and assumes that the actuators are sources of force. Initial studies on impedance control of a high-performance hydraulic joint driven by a hydraulic motor with a jet pipe servovalve [2], and of a single-dof hydraulic servo [4], have been presented. Further, impedance controllers have been studied and implemented on teleoperated hydraulic servosystems for heavy duty works, i.e., backhoe excavators, [10, 25]. The control of excavator-based machines is still primitive and not servo-based; therefore the position control has not got the required accuracy yet, and a rather poor performance is obtained. Moreover, in [25] the hydraulic model is not included.

In this paper, a model-based impedance controller for a 6-dof electrohydraulic Stewart platform is developed. Rigid body and experimentally developed electrohydraulic models, including servovalve, friction and leakage models are employed and described by a set of integrated system equations. Despite the fact that an electrohydraulic servoactuator is not a source of force, as is the case with electric actuators, a novel impedance controller is developed. This controller computes servovalve currents and consists of a feedback and a model-based feedforward loop. An impedance filter modifies the desired trajectory according to a specified behavior. This trajectory is fed to a system model in the controller aiming to reduce the effects of the nonlinear hydraulic dynamics. Simulations results compare system response of the developed and of a proportional-derivative (PD) controller for electrohydraulic systems. It is shown that during interactions with the environment, the impedance controller is superior to PD controllers, while its response is smooth.

2. System Modeling

An electrohydraulic Stewart platform servomechanism is a 6-dof closed kinematic chain mechanism consisting of a fixed base and a moving platform, with six hydraulic actuators supporting it, see Fig. 1. In this section, the dynamic model of a Stewart platform is developed.

2.1. Mechanical Dynamics

The rigid body equations of motion for a Stewart platform are derived using a Lagrangian formulation and are in the following form,

$$\mathbf{M}(\mathbf{x})\ddot{\mathbf{x}} + \mathbf{V}(\mathbf{x}, \dot{\mathbf{x}}) + \mathbf{G}(\mathbf{x}) + \mathbf{F}_{fr}(\dot{\mathbf{x}}) = \tau \qquad (1)$$

where $\mathbf{x} = (x_0, y_0, z_0, p, q, r)^{\mathrm{T}}$ is the 6×1 vector of the platform generalized coordinates, see Fig. 1. The x_0, y_0, z_0, are the platform center of mass (CM) Cartesian coordinates, p, q, r are the platform Euler angles, $\mathbf{M}(\mathbf{x})$ is the 6×6 positive definite mass matrix of the system, $\mathbf{V}(\mathbf{x}, \dot{\mathbf{x}})$ is a 6×1 vector that includes centrifugal and Coriolis forces/torques, $\mathbf{G}(\mathbf{x})$ is a 6×1 vector that includes forces/torques due to gravity, $\mathbf{F}_{fr}(\dot{\mathbf{x}})$ is the 6×1 vector of friction forces/torques, and τ is the 6×1 vector of the generalized applied forces.

The generalized applied forces can be written as a function of the hydraulic actuator forces, [27],

$$\tau = \mathbf{J}^T \mathbf{F}_p, \qquad (2)$$
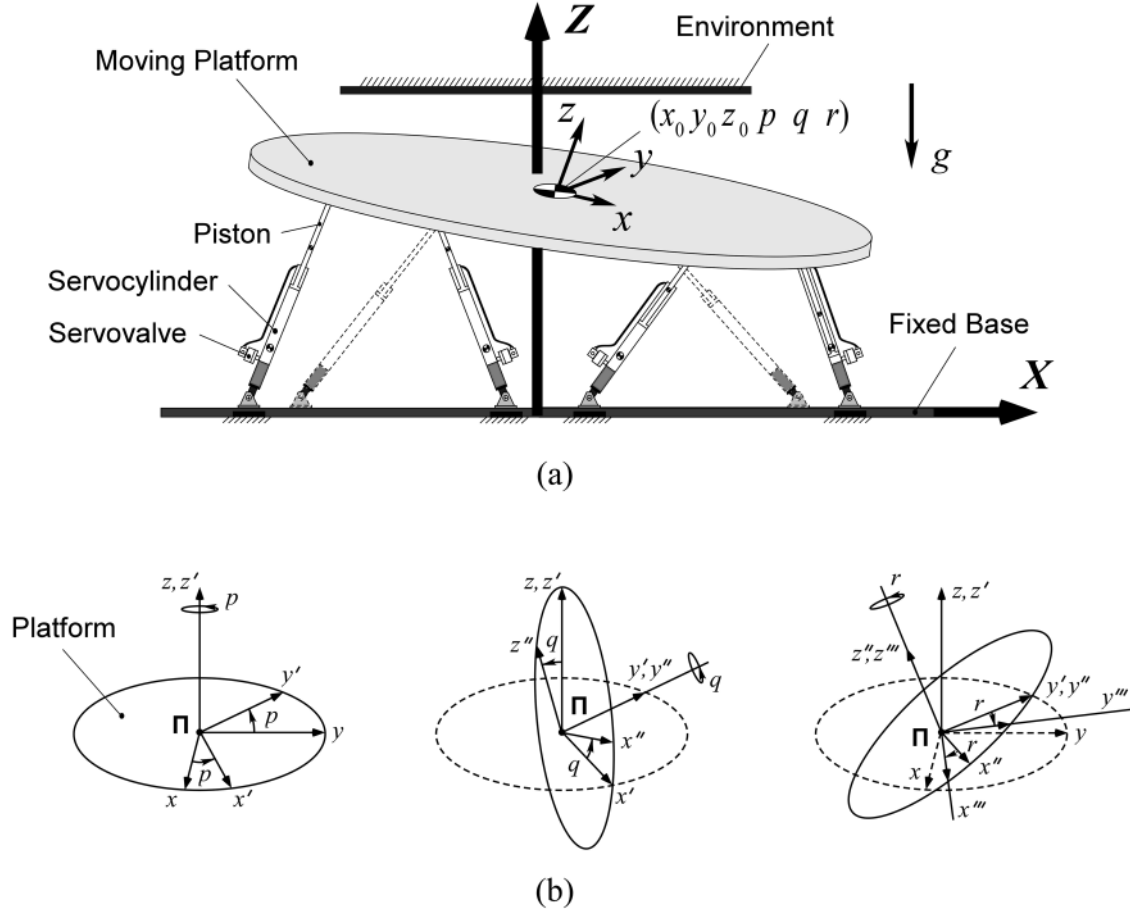
Fig. 1. (a) Schematic view of a six-dof Stewart platform, (b) orientation of moving platform.

where $\mathbf{J}$ is the overall Jacobian 6×6 matrix of the platform, and $\mathbf{F}_p$ is a 6×1 vector representing actuator forces given by,

$$\mathbf{F}_p = \left(F_{p,1}, F_{p,2}, \ldots, F_{p,6} \right)^{\mathrm{T}}, \tag{3}$$

where $F_{p,j}$, $j = 1, 2, \ldots, 6$ are individual hydraulic forces acting on the platform.

Using mechanism differential kinematics, see Appendix A, and Eq. (2), Eq. (1) is transformed to its joint space and written as,

$$\mathbf{M}^*(\mathbf{x})\ddot{\ell} + \mathbf{V}^*(\mathbf{x}, \dot{\mathbf{x}}) + \mathbf{G}^*(\mathbf{x}) + \mathbf{F}_{fr}^*(\dot{\ell}) = \mathbf{F}_p, \tag{4}$$

where $\ell = (\ell_1, \ell_2, \ldots, \ell_6)^{\mathrm{T}}$ is the 6×1 vector of actuator displacements, $\mathbf{M}^*(\mathbf{x})$ is a 6×6 positive definite mass matrix, $\mathbf{V}^*(\mathbf{x}, \dot{\mathbf{x}})$ is a 6×1 vector that contains the centrifugal and Coriolis forces, $\mathbf{G}^*(\mathbf{x})$ is a 6×1 gravity forces vector, and $\mathbf{F}_{fr}^*(\dot{\ell})$ is a 6×1 vector that contains joint space frictional forces. The terms

$\mathbf{M}^*(\mathbf{x})$, $\mathbf{V}^*(\mathbf{x}, \dot{\mathbf{x}})$ and $\mathbf{G}^*(\mathbf{x})$ are given, respectively by (see Appendix A),

$$\mathbf{M}^*(\mathbf{x}) = [\mathbf{J}(\mathbf{x})^{\mathrm{T}}]^{-1}\mathbf{M}(\mathbf{x})\,\mathbf{J}(\mathbf{x})^{-1} \tag{5a}$$

$$\mathbf{V}^*(\mathbf{x}, \dot{\mathbf{x}}) = [\mathbf{J}(\mathbf{x})^{\mathrm{T}}]^{-1} [\mathbf{V}(\mathbf{x}, \dot{\mathbf{x}}) - \mathbf{M}(\mathbf{x})\,\dot{\mathbf{J}}(\mathbf{x}, \dot{\mathbf{x}}) \cdot \dot{\mathbf{x}}] \tag{5b}$$

$$\mathbf{G}^*(\mathbf{x}) = [\mathbf{J}(\mathbf{x})^{\mathrm{T}}]^{-1}\mathbf{G}(\mathbf{x}) \tag{5c}$$

A number of methods exists, that can be used to model friction [12]. A widely accepted method models friction $\mathbf{F}_{fr}^*(\dot{\ell})$, as,

$$\mathbf{F}_{fr}^*(\dot{\ell}) = \mathbf{F}_v^*(\dot{\ell}) + \mathbf{F}_c^*(\dot{\ell}) + \mathbf{F}_s^*, \tag{6}$$

where $\mathbf{F}_v^*(\dot{\ell})$, $\mathbf{F}_c^*(\dot{\ell})$ and $\mathbf{F}_s^*$ are the viscous, Coulomb and static friction vectors, with elements,

$$F_{v,j}^*(\dot{\ell}_j) = \begin{cases} 0, & \dot{\ell}_j = 0, \quad j = 1, 2, \ldots, 6 \\ b_j\dot{\ell}_j, & \dot{\ell}_j \neq 0, \quad j = 1, 2, \ldots, 6 \end{cases} \tag{7a}$$

$$F^*_{c,j}(\dot{\ell}_j) = \begin{cases} 0, & \dot{\ell}_j = 0, \quad j = 1, 2, \ldots, 6 \\ F_{c0,j}\, sgn(\dot{\ell}_j), & \dot{\ell}_j \neq 0, \quad j = 1, 2, \ldots, 6 \end{cases}$$

(7b)

$$F^*_{s,j} = \begin{cases} F_{ext,j}, & |F_{ext,j}| < F_{s0,j}, \dot{\ell}_j = 0, \ddot{\ell}_j = 0, \\ & j = 1, 2, \ldots, 6 \\ F_{s0,j}\, sgn(F_{ext,j}), & |F_{ext,j}| > F_{s0,j}, \dot{\ell}_j = 0, \ddot{\ell}_j \neq 0, \\ & j = 1, 2, \ldots, 6 \\ 0, & \dot{\ell}_j \neq 0, \\ & j = 1, 2, \ldots, 6 \end{cases}$$

(7c)

where b_j is the jth parameter for the viscous friction element, $F_{c0,j}$ is the jth parameter for the Coulomb friction element, $F_{ext,j}$ is the jth external force element, $F_{s0,j}$ is the jth breakaway force element, and

$$sgn(\dot{\ell}_j) = \begin{cases} +1, & \dot{\ell}_j > 0, \quad j = 1, 2, \ldots, 6 \\ 0, & \dot{\ell}_j = 0, \quad j = 1, 2, \ldots, 6 \\ -1, & \dot{\ell}_j < 0, \quad j = 1, 2, \ldots, 6 \end{cases}$$

(8)

2.2. Hydraulic Dynamics

The electrohydraulic actuation servosystem of the platform consists of pistons, servovalves, controllers, sensors and a hydraulic power supply. Models of the major components are introduced next.

Servo hydraulic supplies include constant pressure piston pumps, driven by induction electric motors. Therefore, the pump is modeled as a constant pressure source. Supplies may also include accumulators for filtering pressure pulsations from the pump, and for allowing the use of smaller rating pumps by providing additional flow when needed. Such an accumulator, is modeled as a hydraulic capacitor [20].

A single rod hydraulic servocylinder is illustrated schematically in Fig. 2. The equations relating mechanical to hydraulic variables are described by,

$$Q_1 = A_1\dot{\ell} + C_1\dot{P}_1 + G_{p,in}(P_1 - P_2)$$

(9a)

$$Q_2 = A_2\dot{\ell} - C_2\dot{P}_2 + G_{p,in}(P_1 - P_2)$$

(9b)

$$A_1 P_1 - A_2 P_2 = F_p$$

(9c)

$$F_{act} = F_p - F_{fr,p},$$

(9d)

where Q_1, Q_2 are the flows through the two cylinder chamber ports, P_1, P_2 are the chamber pressures, A_1 is the piston side area, A_2 is the rod side area, C_1, C_2 are the fluid capacitances in the cylinder chambers, (modeling fluid compressibility), $G_{p,in}$ represents cylinder internal leakage conductance, ℓ is the total length of actuator, F_p is the hydraulic force, $F_{fr,p}$ is the actuator friction force, and F_{act} is the net actuator output force. In the case of a hydraulic cylinder with a double rod, the two areas A_1 and A_2 are equal and therefore, Eq. (9) are simplified.
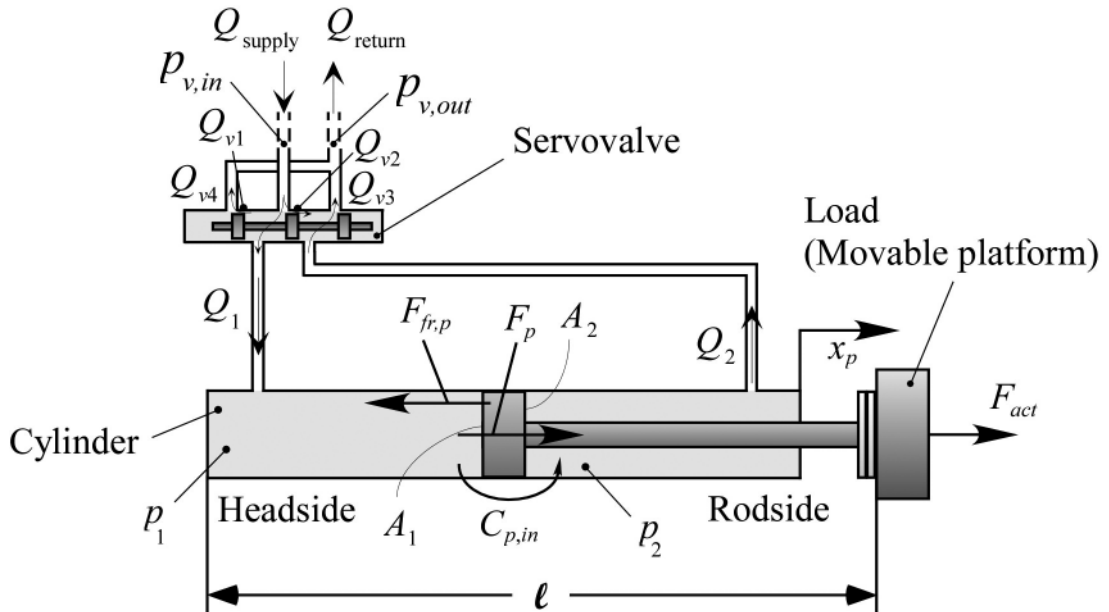
Fig. 2. Schematic model of a hydraulic servoactuator.

Control of a hydraulic servo is achieved through the use of servovalves, see Fig. 3a. Since their natural frequency is much higher than that of the mechanical load, only the valve resistive effect is considered here. It is also assumed that the valve geometry is ideal, e.g., the valve has sharp edges and zero cross leakage, [3,26].

A high-performance critical center hydraulic servovalve consists of four symmetric and matched servovalve orifices making up flow paths through four nonlinear fluid resistors, modulated by the input voltage, see Fig. 3a. Thereby, the servovalve is modeled as the hydraulic equivalent of a Wheatstone bridge, see Fig. 3b. When the servovalve input current is positive, $i > 0$, flow passes through the orifices 1 and 3 (path $P - A - B - T$), while flow leakages pass through valve orifices 2 and 4. Similarly, when the servovalve input current is negative, $i < 0$, flow passes through the path $P - A - B - T$, and flow leakages through orifices 1 and 3. This model is described analytically by,

$$Q_{v1} = C_{G_1}(i, C_d, \rho)\sqrt{\Delta P_{G_1}} \tag{10a}$$

$$Q_{v2} = C_{G_2}(i, C_d, \rho)\sqrt{\Delta P_{G_2}} \tag{10b}$$

$$Q_{v3} = C_{G_3}(i, C_d, \rho)\sqrt{\Delta P_{G_3}} \tag{10c}$$

$$Q_{v4} = C_{G_4}(i, C_d, \rho)\sqrt{\Delta P_{G_4}} \tag{10d}$$

where i is the servovalve current (control input), ΔP_{G_j} is the pressure drop across, Q_{v_j} is the servovalve flow through orifice j, $(j = 1, \ldots, 4)$, $C_{G_j}(i, C_d, \rho)$, is a nonlinear function in the servovalve motor current, the discharge coefficient, C_d, and the mass density of the fluid, $\rho, (j = 1, \ldots, 4)$. In general, the discharge coefficient is a function of the Reynolds number and valve geometry. However, fluid density and Reynolds dependencies are weak for turbulent flow and therefore only the current dependency is significant here, [17]. In addition, because of servovalve symmetry, the C_G functions are given by the following equations, depending on the sign of the current i,

- If $i > 0$, the main flow path passes through the orifices 1 and 3, see Fig. 3b, and,

$$C_{G_1}(i) = C_{G_3}(i) \equiv C_{G_{sv,main}}(i) \tag{11a}$$

$$C_{G_2}(i) = C_{G_4}(i) \equiv C_{G_{sv,leak}}(i) \tag{11b}$$

- If $i < 0$, the main flow path passes through the orifices 2 and 4, see Fig. 3b, and,

$$C_{G_2}(i) = C_{G_4}(i) \equiv C_{G_{sv,main}}(-i) \tag{12a}$$

$$C_{G_1}(i) = C_{G_3}(i) \equiv C_{G_{sv,leak}}(-i) \tag{12b}$$

where $C_{G_{sv,main}}$ and $C_{G_{sv,leak}}$ represent current functions for the main and leakage flows of the servovalve, respectively.

In previous works, servovalve behavior was neglected or was studied using a linearized analysis about a particular operating point, [17]. However, we have found that the servovalve model is of critical
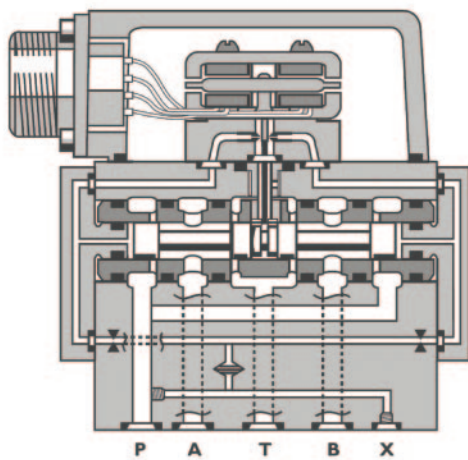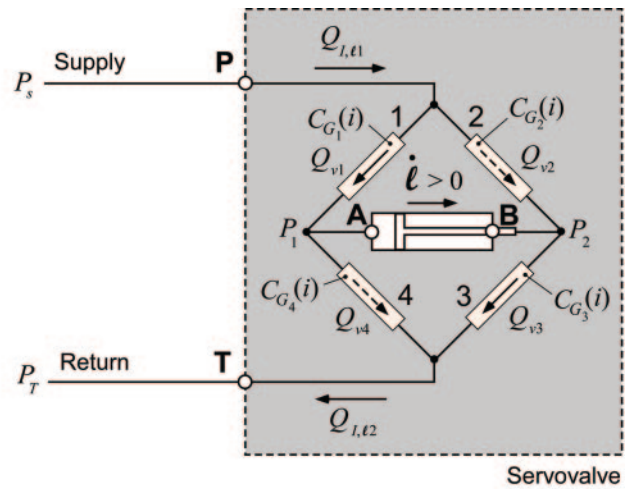
Fig. 3. (a) Cutout of a servovalve, (b) schematic model of servovalve.

importance to the controller performance. A fair, but not accurate enough, servovalve model was employed in our previous work, in which the servovalve orifice functions $C_{G_j}(j = 1, \ldots, 4)$ were linear with respect to the current, [5]. Fig. 4a displays the servovalve current when a linear valve model is used; inaccurate peaks of numerical nature appear when the valve closes or opens.

To avoid these problems, we introduce here a valve nonlinear model. Based on our experimental work, a good approximation of the current functions for the main and leakage flows of the servovalve, see Eqs. (11) and (12), is given by second- and third-order polynomials, as follows,

$$
C_{G_{sv,main}}(i) = \begin{cases} K_{1,main}i + K_{0,main}\,, \\ \qquad\qquad\qquad |i| > i_{0,main} \\ k_{2,main}i|i| + k_{1,main}\,i + k_0\,, \\ \qquad\qquad\qquad |i| < i_{0,main} \end{cases} \tag{13a}
$$

$$
C_{G_{sv,leak}}(i) = \begin{cases} K_{0,leak}\,, \qquad\qquad\quad |i| > i_{0,leak} \\ k_{3,leak}i^3 + k_{2,leak}i|i| + k_{1,leak}\,i + k_0\,, \\ \qquad\qquad\qquad\qquad |i| < i_{0,leak} \end{cases}
$$
$$\tag{13b}$$

where the coefficients $K_{1,main}$, $K_{0,main}$ and $K_{0,leak}$ are positive constant parameters, and the coefficients $k_{1,main}$, $k_{2,main}$, $k_{1,leak}$, $k_{2,leak}$, $k_{3,leak}$ and k_0 are constant parameters. The $i_{0,main}$, $i_{0,leak}$ are characteristic threshold servovalve current values, for the main and leakage valve paths, respectively. With this model, the peaks in Fig. 4a are eliminated completely and the transition from opening to closing of the valve is smooth, see Fig. 4b (areas B). To estimate the coeffi-

cients in Eq. (13), a least squares analysis method using data from an experimental 1-dof electro-hydraulic servosystem was employed. The resulting functions for a two-land-four-way spool Moog G761–3004 Series high-performance servovalve are illustrated in Fig. 5. The values of the identified valve parameters are shown in Table 1.

Hydraulic hoses are modeled as compressible hydraulic lines, [20]. The equations that describe the hose dynamics are given by,

$$
P_{C,\ell_{in}} - P_{C,\ell_{out}} = I\dot{Q}_{\ell,out} + RQ_{\ell,in} \tag{14a}
$$

$$
(\dot{P}_{C,\ell_{in}} - R\dot{Q}_{\ell,in})C = Q_{\ell,in} - Q_{\ell,out} \tag{14b}
$$

where $P_{C,\ell_{in}}$ and $P_{C,\ell_{out}}$ are hose pressures at the input and output point, respectively, $Q_{\ell,in}$ and $Q_{\ell,out}$ are the flows through the hose at its input and output correspondingly, and R, I, C are the hose resistance, inertance and capacitance, respectively.

2.3. Integrated System Equations

The hydraulic and mechanical load dynamics of the platform are described by the integrated system equations derived using a systems approach, such as the Linear Graph, [20], or Bond Graph methods, [19]. To this end, one needs to provide expressions transforming pressure differences to forces, see Eq. (9c), and velocities to flows, see Eq. (9a,b).

Here, the Linear Graph method is employed, [20]. The linear graph of the full model of the 6-dof hydraulic servosystem is depicted in Fig. 6. The application of continuity and compatibility laws, along with individual element equations, leads to a set
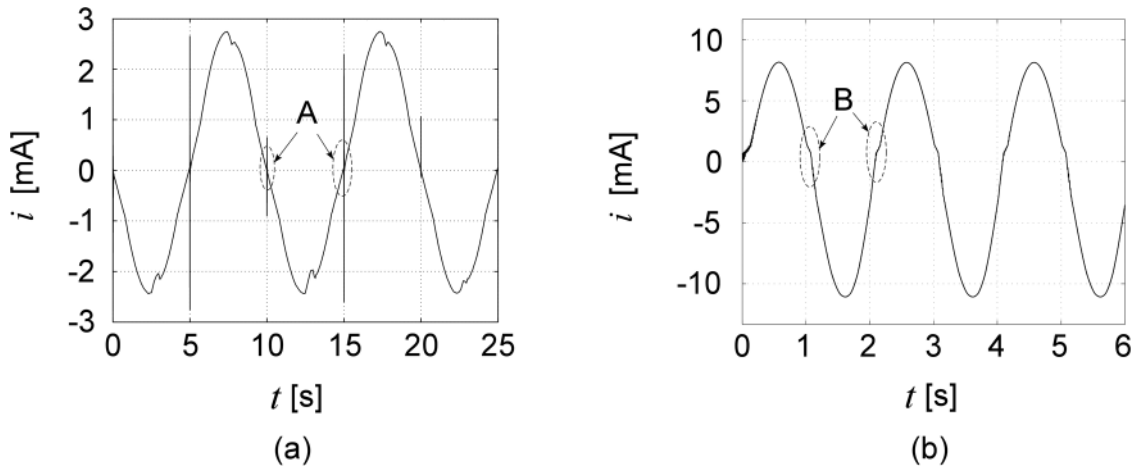
Fig. 4. Servovalve current response using (a) a linear model, (b) a nonlinear model.
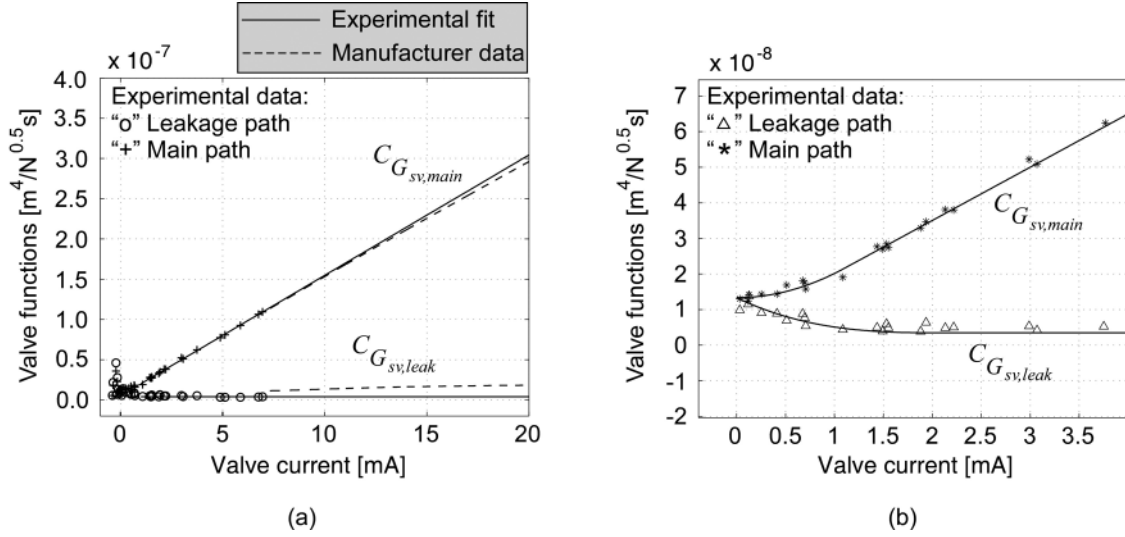
Fig. 5. (a) Experimental valve functions in main and leakage path for a Moog G761-3004 Series high-performance servovalve (b) zoom in the nonlinear valve functions-valve current area.

Table 1. Experimental values of the Moog G761-3004 servovalve parameters

Servovalve parameter	Value
$K_{1,main}$	$1.50 \times 10^{-5}\,\mathrm{m^{7/2}/(A\,kg^{1/2})}$
$K_{0,main}$	$5.13 \times 10^{-9}\,\mathrm{(m^7/kg)^{1/2}}$
$k_{1,main}$	0
$k_{2,main}$	$6.80 \times 10^{-3}\,\mathrm{m^{7/2}/(A^2\,kg^{1/2})}$
k_0	$1.34 \times 10^{-8}\,\mathrm{(m^7/kg)^{1/2}}$
$k_{0,leak}$	$3.48 \times 10^{-9}\,\mathrm{(m^7/kg)^{1/2}}$
$k_{1,leak}$	$-1.32 \times 10^{-5}\,\mathrm{m^{7/2}/(A\,kg^{1/2})}$
$k_{2,leak}$	$5.81 \times 10^{-3}\,\mathrm{m^{7/2}/(A^2\,kg^{1/2})}$
$k_{3,leak}$	$-0.84\,\mathrm{m^{7/2}/(A^3\,kg^{1/2})}$
$i_{0,main}$	1mA
$i_{0,leak}$	1.5mA

of 48 nonlinear first-order differential equations, as follows,

$$\dot{P}_{1,j} = \frac{1}{C_1} \cdot [Q_{I,\ell 1} - Q_{v2}(i) - Q_{v4}(i) - G_{p,in} \cdot (P_1 - P_2) - A_1 v]\big|_j, \; j = 1, 2, \ldots, 6$$
(15a)

$$\dot{P}_{2,j} = \frac{1}{C_2} \cdot [Q_{v2}(i) + Q_{v4}(i) - Q_{I,\ell 2} + G_{p,in} \cdot (P_1 - P_2) + A_2 v]\big|_j, \; j = 1, 2, \ldots, 6$$
(15b)

$$\dot{P}_{C,\ell 1,j} = \frac{1}{C_{\ell 1}} \cdot [\frac{R_{\ell 1}}{P_s - P_{C,\ell 1}} - Q_{I,\ell 1}]\big|_j, \; j = 1, 2, \ldots, 6$$
(15c)

$$\dot{P}_{C,\ell 2,j} = \frac{1}{C_{\ell 2}} \cdot [Q_{I,\ell 2} - \frac{R_{\ell 2}}{P_{C,\ell 2} - P_T}]\big|_j, \; j = 1, 2, \ldots, 6$$
(15d)

$$\dot{Q}_{I,\ell 1,j} = \frac{1}{I_{\ell 1}} \cdot [P_{C,\ell 1} - P_1 - \Delta P_{G_1}(i)]\big|_j, \; j = 1, 2, \ldots, 6$$
(15e)

$$\dot{Q}_{I,\ell 2,j} = \frac{1}{I_{\ell 2}} \cdot [P_2 - P_{C,\ell 2} - \Delta P_{G_3}(i)]\big|_j, \; j = 1, 2, \ldots, 6$$
(15f)

$$\dot{v}_j = [\mathbf{m}_-^*]\big|_j \cdot (\mathbf{F}_p - \mathbf{V}^* - \mathbf{G}^* - \mathbf{F}_{fr}^*), \; j = 1, 2, \ldots, 6$$
(15g)

$$\dot{\ell}_j = v_j,$$
(15h)

where $Q_{I,\ell 1,j}$, $Q_{I,\ell 2,j}$ are the jth flows in the jth hydraulic pressure and return line correspondingly, P_s, P_T are the power supply and return pressure of the servo-system, respectively, $P_{C,\ell 1,j}$, $P_{C,\ell 2,j}$ are correspondingly the jth pressures of jth hydraulic power and return line regarding with the lines' capacitances, $I_{\ell 1,j}$, $R_{\ell 1,j}$, $C_{\ell 1,j}$ are the jth inertance, resistance and capacitance of jth hydraulic power line respectively, $I_{\ell 2,j}$, $R_{\ell 2,j}$, $C_{\ell 2,j}$ are the jth inertance, resistance and capacitance of jth hydraulic return line respectively, v_j is the velocity of the jth piston, which corresponds to the jth element of the vector, and $[\mathbf{m}_-^*]\big|_j$ is a 1×6 row-matrix which
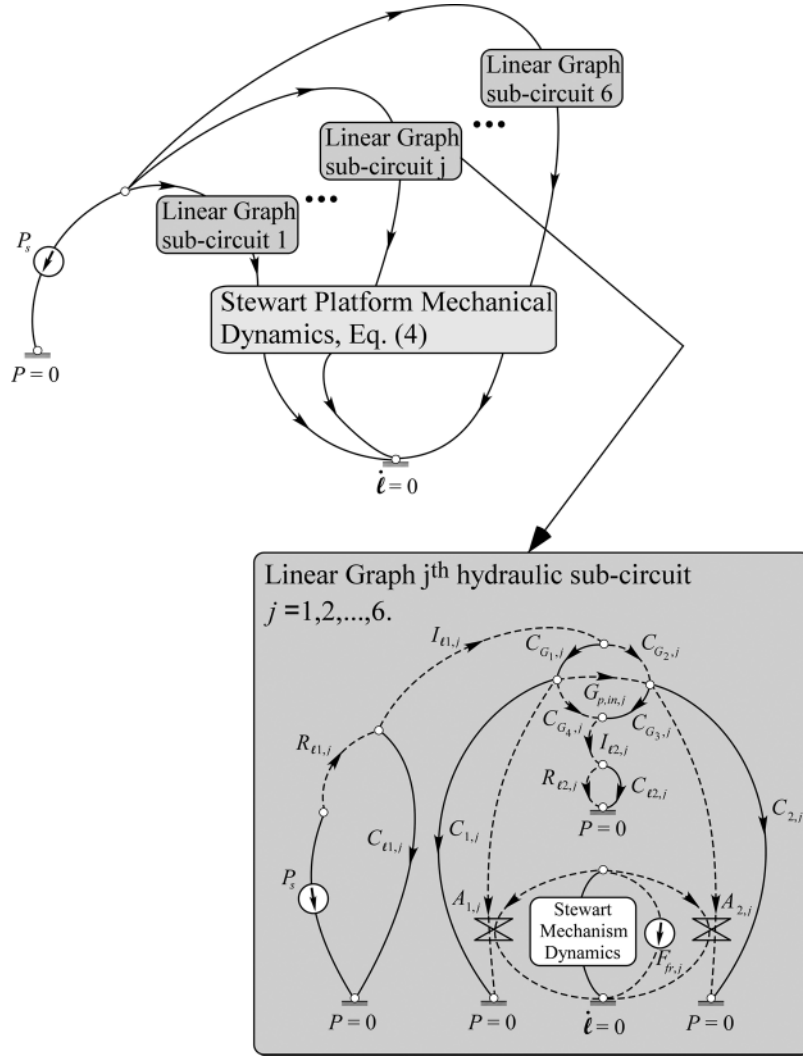
Fig. 6. Full linear graph of the 6-dof electrohydraulic Stewart platform.

corresponds to the jth line of the matrix $(\mathbf{M}^*)^{-1}$. Finally, $\Delta P_{G_1}(i)|_j$, $\Delta P_{G_3}(i)|_j$ are the jth pressure drops of the jth servovalve orifices 1 and 3, respectively.

These are determined using the flow continuity laws, along with actuator and servovalve elements equations, see Appendix B, and are given by,

$$\Delta P_{G_1}(i)|_j = \left(\frac{Q_{I,\ell 1} C_{G_1}(i) - C_{G_2}(i)\sqrt{Q_{I,\ell 1}^2 + [C_{G_1}^2(i) - C_{G_2}^2(i)] \cdot (P_1 - P_2)}}{C_{G_1}^2(i) - C_{G_2}^2(i)} \right)^2 \Bigg|_j, \quad j = 1, \ldots, 6 \tag{16a}$$

$$\Delta P_{G_3}(i)|_j = \left(\frac{Q_{I,\ell 2} C_{G_3}(i) - C_{G_4}(i)\sqrt{Q_{I,\ell 2}^2 + [C_{G_3}^2(i) - C_{G_4}^2(i)] \cdot (P_1 - P_2)}}{C_{G_3}^2(i) - C_{G_4}^2(i)} \right)^2 \Bigg|_j, \quad j = 1, \ldots, 6 \tag{16b}$$

Note that due to servovalve symmetry, see Eqs. (11) and (12), the current functions C_{G_1} and C_{G_2}, as well as C_{G_3} and C_{G_4} are not be equal for the same current i, and therefore the functions in Eq. (16) exist always. Further, the flows $Q_{v2}(i)$ and $Q_{v4}(i)$ in Eq. (15a,b) are given by continuity as,

$$Q_{v2,j}(i) = \left[Q_{I,\ell 1} - C_{G_1}(i) \sqrt{\Delta P_{G_1}(i)} \right]\Big|_j, \; j = 1, 2, \dots, 6 \tag{17a}$$

$$Q_{v4,j}(i) = \left[Q_{I,\ell 2} - C_{G_3}(i) \sqrt{\Delta P_{G_3}(i)} \right]\Big|_j, \; j = 1, 2, \dots, 6. \tag{17b}$$

The actuator displacements $x_{p,j}$ and velocities $v_{p,j}$ represent system outputs, which are determined by integrating twice Eq. (15g) and once Eq. (15h), respectively.

3. Impedance Controller Design

In systems actuated by electric motors, actuator Lorentz forces are proportional to actuator currents. This simplifies control laws and allows one to achieve second-order error dynamics converging exponentially to zero. However, such a relationship between force and current does not exist in electrohydraulic systems. Here, a relationship of servovalve currents, in analytical form is achieved, using an impedance model-based control design.

In this section, an impedance model-based control design for a 6-dof electrohydraulic Stewart platform is developed. Impedance control essentially allows a physical system to emulate a simpler one, under the assumption that the desired behavior is within the capabilities of the physical system. An impedance controller serves to keep interaction forces well-behaved, without the need for switching algorithms. In designing an impedance controller, we are interested in the following: (i) forces should be limited, (ii) no consecutive collisions should result, (iii) no contact instability and (iv) there must be a method for achieving these by adjusting the controller gains.

The developed controller computes servovalve currents and consists of (i) model-based feedforward part and (ii) a feedback loop part. The model-based part helps in producing the proper inputs without the need for large feedback gains. In the proposed impedance model-based controller, a new trajectory is computed using an impedance filter. It serves as a new command to an inner position control loop and keeps the system from undesired interactions with the environment. The control design uses the integrated system dynamic and hydraulic models; therefore, it is assumed that $\mathbf{M}^*(\mathbf{x}), \mathbf{V}^*(\mathbf{x}, \dot{\mathbf{x}}), \mathbf{G}^*(\mathbf{x})$, and $\mathbf{F}^*_{fr}(\dot{\ell})$, in Eq. (4), are known.

3.1. Feedforward Control Part

In the feedforward control part, a new desired trajectory that accommodates interaction forces is computed and derived by an impedance filter. The 6×1 servovalve current vector must be determined such that the physical plant behaves like the desired one in both the noncontact and contact regimes. Schematically, the feedforward controller is depicted in Fig. 7. The design of this new trajectory includes a set of impedance parameters, which are responsible for the good behavior of the tracking performance. A typical response system behavior is given by a second-order system, [13].

Here, the output of the impedance filter approach, ℓ_e, chosen for the electrohydraulic platform, depends on feedback of the interaction forces with the environment and is determined from,
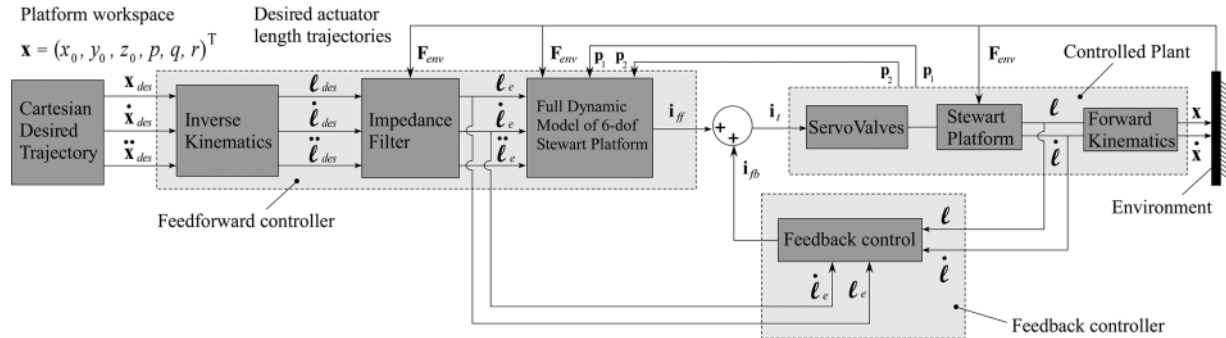
Fig. 7. The impedance model-based controller block diagram of the 6-dof electrohydraulic Stewart servomechanism.

$$\mathbf{M}_{des}(\ddot{\ell}_e - \ddot{\ell}_{des}) + \mathbf{B}_{des}(\dot{\ell}_e - \dot{\ell}_{des}) + \mathbf{K}_{des}(\ell_e - \ell_{des}) = \mathbf{F}_{env}, \tag{18}$$

where $\mathbf{M}_{des}$ is the desired 6×6 inertia matrix, and $\mathbf{B}_{des}$, $\mathbf{K}_{des}$ are the 6×1 damping and stiffness vectors, respectively (i.e., desired impedance matrix and vector parameters) describing the desired second-order behavior, ℓ_e is the 6×1 impedance desired trajectory vector as given by the impedance filter, which depends on the desired one, ℓ_{des}, and the contact force, and $\mathbf{F}_{env}$ is a 6×1 environment force vector acting on the system, which can be measured by a force sensor and approximated by,

$$\mathbf{F}_{env} = \mathbf{K}_{env}(\ell_{env} - \ell) \tag{19}$$

In the above equation, $\mathbf{K}_{env}$ is a diagonal 6×6 environment stiffness matrix with positive elements, and ℓ_{env} is a 6×1 vector, which represents a virtual point of the environment. The desired behavior can be extended considering the virtual point position as a time function and including the velocity, acceleration and force error in the control law scheme, in general. To compute desired actuator length trajectories from desired Cartesian trajectories of the moving platform, the feedforward controller uses the mechanism inverse kinematics, given in Appendix C.

Next, we focus our attention in finding a simplified relationship between servovalve current and piston accelerations. This is achieved using a reduced hydraulic model, in which the leakage flows and the cylinder chamber compressibility are neglected. Thereafter, the flows through the orifices of the servovalve described by Eq. (10a,c) are equal to the flows through cylinder chamber ports, see Eq. 9a,b, and are written as,

$$Q_{v1} = Q_1 = A_1 \dot{\ell} \tag{20a}$$

$$Q_{v3} = Q_2 = A_2 \dot{\ell}. \tag{20b}$$

Further, neglecting the servovalve leakage flows, the pressure drops of the servovalve orifices 1 and 3, see Eq. (16), can be written as,

$$\Delta P_{G_1}(i) = P_s - P_1 \tag{21a}$$

$$\Delta P_{G_3}(i) = P_2 - P_T. \tag{21b}$$

Using Eqs. (10) (11), (12), and (20), the servocylinder chamber pressures are computed as,

$$P_1|_j = \left[P_s - \frac{A_1^2}{C_{G_{sv,main}}^2(i)} \cdot \dot{\ell}_e |\dot{\ell}_e| \right]\Bigg|_j, \quad j = 1, 2, ..., 6 \tag{22a}$$

$$P_2|_j = \left[P_T + \frac{A_2^2}{C_{G_{sv,main}}^2(i)} \cdot \dot{\ell}_e |\dot{\ell}_e| \right]\Bigg|_j, \quad j = 1, 2, ..., 6 \tag{22b}$$

where $\ell_{e,j}$ is the jth element of vector ℓ_e, i_j is the current (control input) for the jth valve/actuator assembly. Combining Eq. (22a,b) is received,

$$[A_1 P_1 - A_2 P_2]|_j = \left[A_1 P_s - A_2 P_T - \frac{A_1^3 + A_2^3}{C_{G_{sv,main}}^2(i)} \cdot \dot{\ell}_e |\dot{\ell}_e| \right]\Bigg|_j, \quad j = 1, 2, ..., 6 \tag{23}$$

The terms $[A_1 P_1 - A_2 P_2]|_j$ are the resulting jth actuator forces, see also Eq. (9c). Eq. (23) is also function of the velocity of the actuators, $\dot{\ell}_{e,j}$. Substituting Eq. (23) in the system equation of motion, Eq. (4), the following equations of motion are derived,

$$\mathbf{M}^*(\mathbf{x})\ddot{\ell}_e + \mathbf{V}^*(\mathbf{x}, \dot{\mathbf{x}}) + \mathbf{G}^*(\mathbf{x}) + \mathbf{F}_{fr}^*(\dot{\ell}_e)$$

$$= \begin{bmatrix} \left[A_1 P_s - A_2 P_T - \frac{A_1^3 + A_2^3}{C_{G_{sv,main}}^2(i)} \cdot \dot{\ell}_e |\dot{\ell}_e| \right]\Big|_1 \\ \cdot \\ \cdot \\ \cdot \\ \left[A_1 P_s - A_2 P_T - \frac{A_1^3 + A_2^3}{C_{G_{sv,main}}^2(i)} \cdot \dot{\ell}_e |\dot{\ell}_e| \right]\Big|_6 \end{bmatrix}. \tag{24}$$

Solving last equation for $C_{G_{sv,main}}(i)\big|_j$, we obtain,

$$C_{G_{sv,main}}(i)\big|_j = \sqrt{\frac{(A_1^3 + A_2^3) \cdot \dot{\ell}_e |\dot{\ell}_e|}{A_1 P_s - A_2 P_T - F_p}}\Bigg|_j, \quad j = 1, 2, ..., 6 \tag{25}$$

where $F_{p,j}$ is the jth element of vector $\mathbf{M}^*(\mathbf{x})\ddot{\ell}_e + \mathbf{V}^*(\mathbf{x}, \dot{\mathbf{x}}) + \mathbf{G}^*(\mathbf{x}) + \mathbf{F}_{fr}^*(\dot{\ell}_e)$, see Eq. (25). Combining Eqs. (13) and (25) the components of the feedforward servovalve current vector, $\mathbf{i}_{ff} = (i_{ff,1}, \ i_{ff,2}, \dots, i_{ff,6})^T$, are computed as,

$$i_{ff,j} = \begin{cases} \left[\dfrac{\dot{\ell}_e}{K_{1,main}} \cdot \sqrt{\dfrac{A_1^3 + A_2^3}{A_1 P_s - A_2 P_T - F_p}} - \dfrac{K_{0,main}}{K_{1,main}} \right]\Bigg|_j, \\ \qquad i_{ff,j} \geq i_{0,main,j} \geq 0, \quad j = 1, 2, \ldots, 6 \\ \left[\dfrac{-k_{1,main} + \sqrt{\Delta_+}}{2 k_{2,main}} \right]\Bigg|_j, \\ \qquad 0 < i_{ff,j} < i_{0,main,j}, \quad j = 1, 2, \ldots, 6 \\ \left[-\dfrac{\dot{\ell}_e}{K_{1,main}} \cdot \sqrt{\dfrac{A_1^3 + A_2^3}{A_1 P_s - A_2 P_T - F_p}} - \dfrac{K_{0,main}}{K_{1,main}} \right]\Bigg|_j, \\ \qquad i_{ff,j} < -i_{0,main,j} < 0, \quad j = 1, 2, \ldots, 6 \\ \left[\dfrac{-k_{1,main} - \sqrt{\Delta_-}}{2 k_{2,main}} \right]\Bigg|_j, \\ \qquad -i_{0,main,j} < i_{ff,j} < 0, \quad j = 1, 2, \ldots, 6 \end{cases} \tag{26}$$

where

$$\Delta_+|_j \equiv \left\{ k_{1,main}^2 - 4 k_{2,main} \left[k_0 - \dot{\ell}_e \cdot \sqrt{\dfrac{A_1^3 + A_2^3}{A_1 P_s - A_2 P_T - F_p}} \right] \right\}\Bigg|_j,$$
$$j = 1, 2, ..., 6 \tag{27a}$$

$$\Delta_-|_j \equiv \left\{ k_{1,main}^2 - 4 k_{2,main} \left[k_0 + \dot{\ell}_e \cdot \sqrt{\dfrac{A_1^3 + A_2^3}{A_1 P_s - A_2 P_T - F_p}} \right] \right\}\Bigg|_j,$$
$$j = 1, 2, ..., 6 \tag{27b}$$

Eq. (26) corresponds to the impedance model-based feedforward controller that yields the servovalve current vector for a given desired trajectory. The controller includes a model of both the mechanism and the electrohydraulic actuation dynamics. The developed feedforward part requires position, velocity, acceleration, piston chamber pressures, and interaction force feedback and therefore, the corresponding sensors. The difference with controllers for electromechanical systems is that here we require the additional use of pressure sensors. Position and velocity feedback are available, while acceleration terms can be dropped since for the application at hand, they are typically small or even zero (for constant velocity motions).

3.2. Feedback Control Part

A feedback control signal is added to further reduce the effects of parametric uncertainty. The feedback controller computes the feedback servovalve currents,

$i_{fb,j}, \ j = 1, 2, \ldots, 6$, as a function of the impedance desired lengths ℓ_e. This loop can include a number of terms depending on the robustness and performance required. A controller that has been used in the past is the following,

$$\mathbf{i}_{fb} = \mathbf{K}_v (\dot{\ell}_e - \dot{\ell}) + \mathbf{K}_p (\ell_e - \ell) \tag{28}$$

where $\mathbf{i}_{fb}$ is the 6×1 servovalve current vector, K_p and $\mathbf{K}_v$ are 6×6 diagonal matrices, which represent the control gains of the system, and ℓ_e is determined by Eq. (18).

This feedback control law increases the bandwidth with respect to the previous feedforward controller. Position and velocity are required for feedback, see Fig. 7.

3.3. Full Control Scheme

The full control law scheme of the 6-dof servosystem is given by the total 6×1 servovalve current vector of the feedback and feedforward current, that were computed above,

$$\mathbf{i}_t = \mathbf{i}_{fb} + \mathbf{i}_{ff}. \tag{29}$$

We first note that if the feedforward control input is applied to the servovalve, the system behavior is controlled by Eq. (18), which is stable by design, given a proper impedance matrix selection. The feedback loop is meant to eliminate small errors due to modeling errors, noise, etc. This loop is position-based and has been shown to be stable by a number of works, for example [1]. When both loops operate simultaneously, one can show by linearization that the controller is stable. However, showing that the controller is stable in conjunction with the full nonlinear hydraulic system is not trivial and will be addressed in the future.

4. Simulation Results

The tracking performance of the controller is evaluated next. Usually, in Stewart platform mechanisms, the platform mass is much larger than the mass of the actuators. Due to this fact, and to simplify the terms in the equations of motion for the needs of this paper, the terms $\mathbf{M}(\mathbf{x})$, $\mathbf{V}(\mathbf{x}, \dot{\mathbf{x}})$ and $\mathbf{G}(\mathbf{x})$ of Eq. (1) are simplified by neglecting actuator masses. The resulting matrices and vectors, i.e., $\mathbf{M}(\mathbf{x})$, $\mathbf{V}(\mathbf{x}, \dot{\mathbf{x}})$ and $\mathbf{G}(\mathbf{x})$ are given in Appendix D, see Eqs. (D1) – (D3).

The configuration of the 6-dof symmetric Stewart mechanism is illustrated in Fig. 8. The system

parameters are shown in Table 2. The joints of the movable platform and fixed base lie at equal peripheral distances, see Fig. 8. Friction parameters were experimentally computed using a single dof electro-hydraulic servomechanism setup, [5]. According to the identification experimental results shown in Fig. 9, these values are presented in Table 3. Mechanical parametric uncertainties are neglected here, as the controller performance is not sensitive to these.

Simulations runs were obtained using a number of desired trajectories. To compute the control gains, we first require that the response of the piston is critically damped, i.e., $\zeta_j = 1, j = 1, 2, \ldots, 6$. Next, we require a settling time of about $t_s = 1$s, yielding $\omega_j = 2\pi$ rad/s, $j = 1, 2, \ldots, 6$. The matrix gain elements are computed as, $K_{p,j} = 4\pi^2 A/m$, $K_{v,j} = 4\pi As/m, j = 1, 2, \ldots, 6$. The environment stiffness elements are selected as $K_{env,j} = 5 \times 10^4 \text{N/m}$, $j = 1, 2, \ldots, 6$. The desired impedance filter parameters were selected so that the valve current saturation is avoided. According to selection methodology of [2], impedance parameter are selected as, $K_{des,j} = 10^3 \text{N/m}, B_{des,j} = 20\text{Ns/m}$ and $M_{des,j} = 100\text{kg}, j = 1, 2, \ldots, 6$. Finally, the system

natural frequencies were determined by $\omega_{n,j} = \sqrt{K_{des,j}/M_{des,j}} = 3.16$ rad/s, $j = 1, 2, \ldots, 6$.

In Fig. 10, the moving platform is being raised along the Z-axis and a stiff wall is present at $z_{env} = 0.27$ m. The six servoactuators follow the same trajectories because of mechanism symmetry. The piston displacement and velocity responses, the

Table 2. System parameters

System parameter	Value
P_s (supply pressure)	110 bar
P_T (return pressure)	1 bar
A_1 (piston side area)	$2.56 \times 10^{-4} \text{m}^2$
A_2 (rod side area)	$6.41 \times 10^{-4} \text{m}^2$
m (platform mass)	300 kg
I_{xx} (moment of inertia about the platform CM)	25 kgm^2
I_{yy} (moment of inertia about the platform CM)	25 kgm^2
I_{zz} (moment of inertia about the platform CM)	50 kgm^2
r_1 (see Fig. 8)	0.5 m
r_0 (see Fig. 8)	1.0 m
d_1 (see Fig. 8)	0.2 m
d_0 (see Fig. 8)	0.3 m
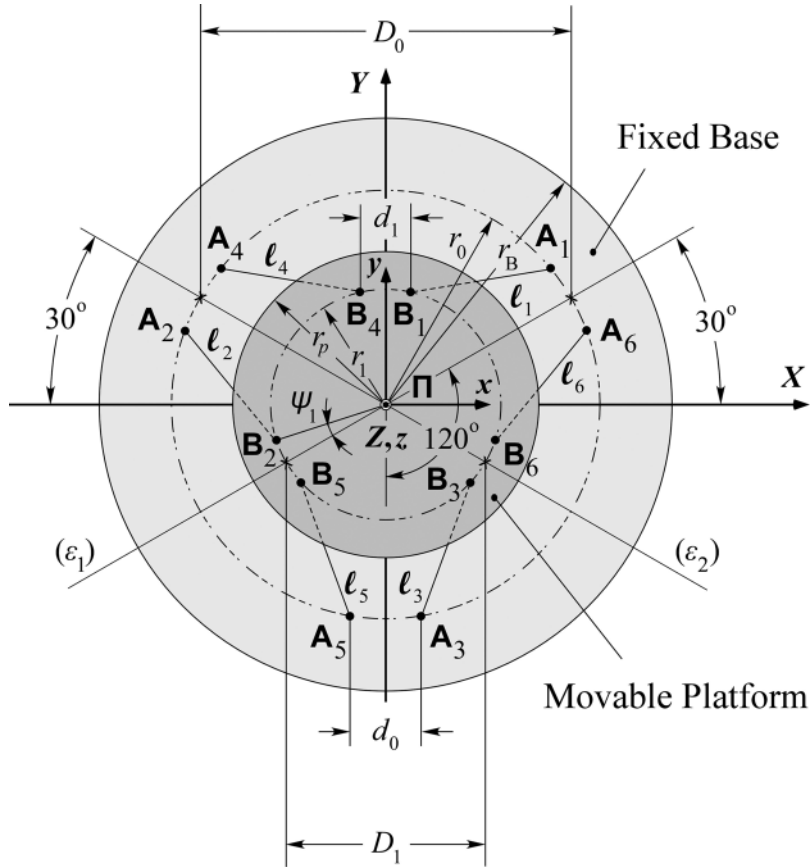
Fig. 8. Assembly configuration of the 6-dof Stewart platform employed.
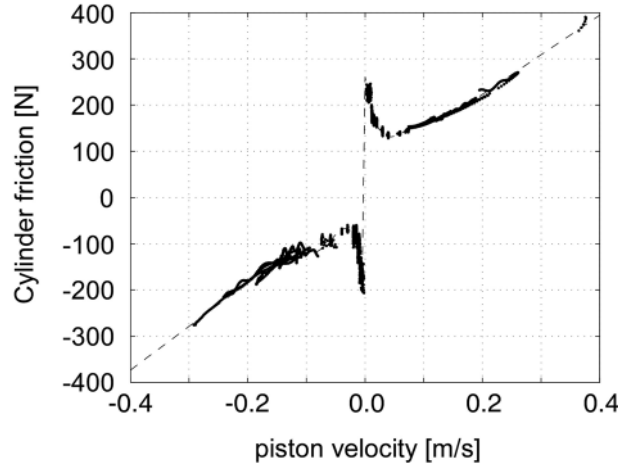
Fig. 9. Experimental results of a hydraulic cylinder friction force vs. piston velocity.

Table 3. Experimental values of servocylinder friction parameters

Friction parameter	Value	
	Piston expansion ($\dot{\ell} > 0$)	Piston compression ($\dot{\ell} > 0$)
b	760.0 Ns/m	945.6 Ns/m
$\left|F_{C,0}\right|$	71.0 N	16.5 N
$\left|F_{s,0}\right|$	245.0 N	210.0 N

environment force response, the input current signals, as well as servoactuator power and chamber pressure histories for the actuators are shown in Fig. 10. As shown in Fig. 10(a), the piston displacements are such that the platform remains in contact with the environment in a controlled way. An expected, steady-state error due to the wall results. The force, after a short transient, settles to a low contact force as expected, see Fig. 10(c). The other system variables exhibit a similar response.

Next, a PD controller is compared to the developed impedance controller assuming a large increase in the payload. For example, we assume that the load is now 30% larger than its true value. The PD control gains are selected such that the maximum control effort between the model-based and the PD algorithms is the same while the damping is critical. Then, the control gains are, $K_{p,j} = 100\pi^2\text{rad}^2/\text{s}^2$, and $K_{v,j} = 20\,\pi\text{rad/s}$, $j = 1, 2, \ldots, 6$. Fig. 11(a,b) shows the results using a PD controller in the case of a ramp response. One can see that a poor position tracking performance is obtained; the PD results in undesirable oscillations while a significant steady-state position error remains. On the other hand, as shown in Fig. 11(c,d), using the impedance model-based controller for the same piston

command, a very good system tracking performance occurs.

Next, the PD and the developed impedance algorithm are compared in the case of erroneous parameter estimation. It is assumed that all joint locations for both the movable platform and fixed base differ by 15% from their true values. These are rather strong assumptions, especially for the kinematic errors, as such platforms are designed at high tolerances for ensuring smoothness of operation. Fig. 12(a,b) shows the results of the PD controller. It is easy to see that a poor position tracking performance is obtained. On the other hand, the robustness of the developed controller is demonstrated in Fig. 12(c,d). Despite these errors, as shown in Fig. 12, the controller leads the system to the desired location in a well-behaved transient. It can be seen that the response is similar to that in which all parameters are known.

It is also interesting to see the controller performance in the case of sensor noise, especially of noise in the pressure sensors. To this end, noise with amplitude equal to 15% of the initial chamber pressure values is added to the pressure measurements. Fig. 13(a) displays the chamber pressures, while Fig. 13(b) the corresponding piston displacement response. Fig. 12(b) shows that the position response remains unaffected in the presence of noise.

The above examples demonstrate that an impedance controller can be developed for an electrohydraulic system, despite the intrinsic nature of the system. Although parameters may not be known exactly, the proposed controller still works in the presence of relatively large parametric uncertainty. Obviously, a better knowledge of the parameters improves the response, and this is to be expected. Reducing parameter uncertainty beyond some
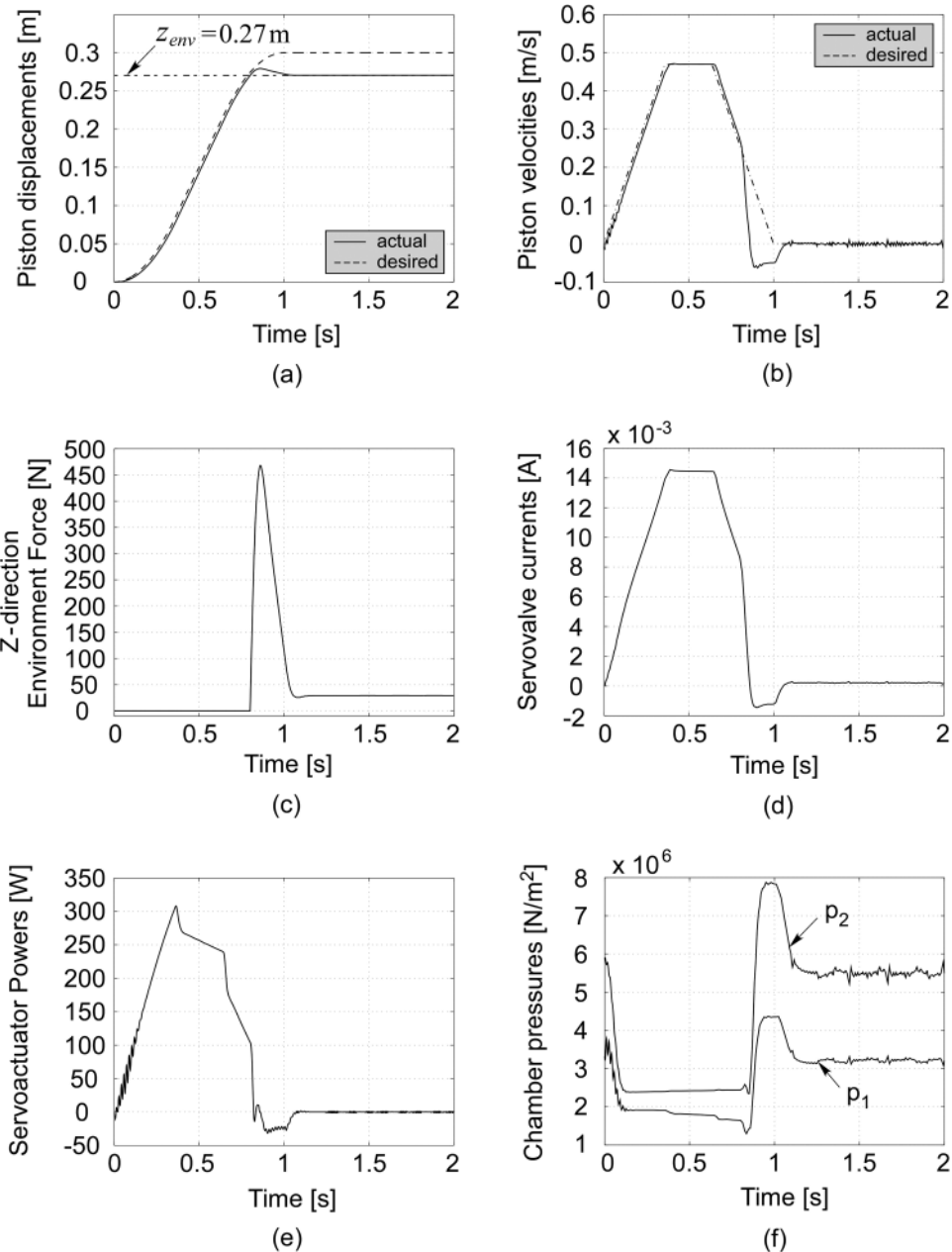
Fig. 10. Simulation results. (a) Piston displacement responses, (b) piston velocity responses, (c) environment force response at Z-direction, (d) input current signals, (e) actuator power history, (f) chamber pressure histories.

threshold requires either the use of a parameter identification method or of an adaptive controller.

5. Conclusions

The development of a novel impedance model-based controller for a 6-6 electrohydraulic Stewart platform with symmetric joint locations was studied. Dynamic models were used that described the rigid body equations of the Stewart platform and the hydraulics

dynamics of its actuation system. Servovalve models and friction were included in the model. The developed control algorithm employed rigid body and actuation dynamics and yielded the servovalve input current vector, in analytical form. The control law consisted of two parts, a feedback and a feedforward one. An impedance filter modified a desired trajectory according to a specified behavior. The modified trajectory was fed to the system model to reduce the effects of the nonlinear hydraulic dynamics. The performance of the developed controller was illustrated
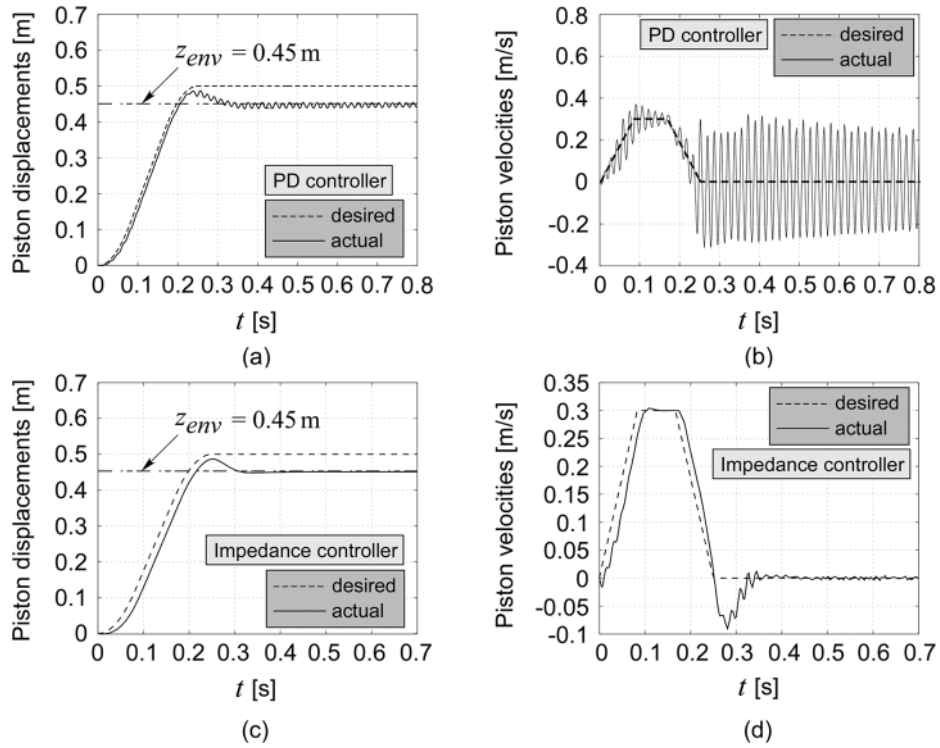
Fig. 11. (a,b) Undesirable oscillations of PD controller with a load increase of 30%; (a) piston displacement responses, (b) piston velocity responses. (c,d) A very good tracking performance of impedance model-based controller with a load increase of 30%; (c) piston displacement responses, (d) piston velocity responses.
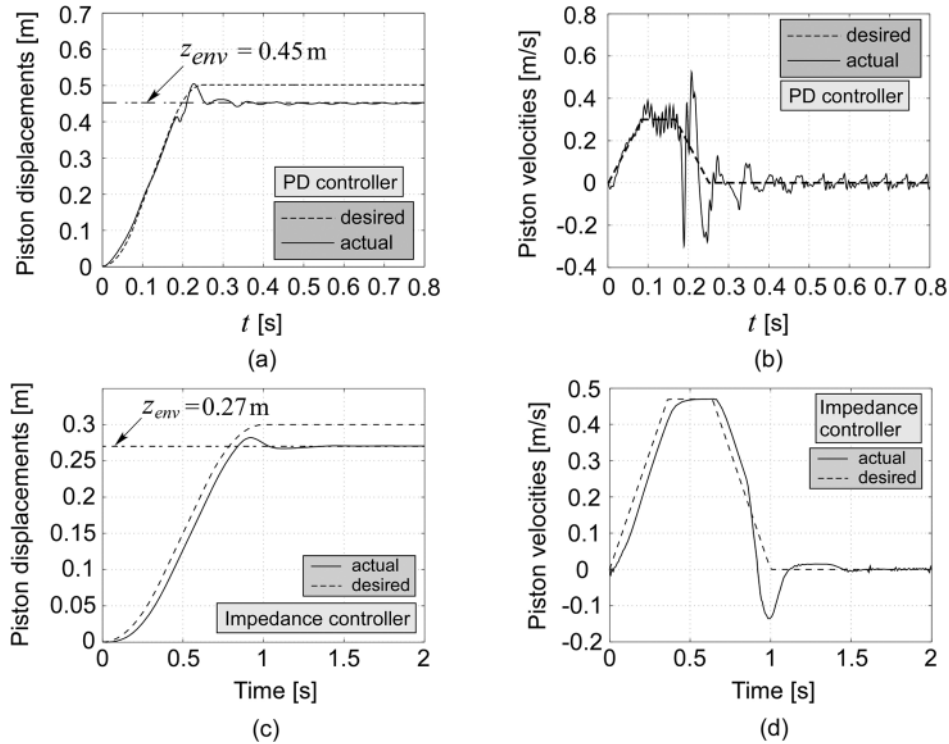
Fig. 12. (a,b) Undesirable system response of PD controller with a parametric error of $\pm 15\%$; (a) piston displacement responses, (b) piston velocity responses. (c,d) Robustness demonstration of impedance model-based controller with a parametric error of $\pm 15\%$; (c) piston displacement responses, (d) piston velocity responses.
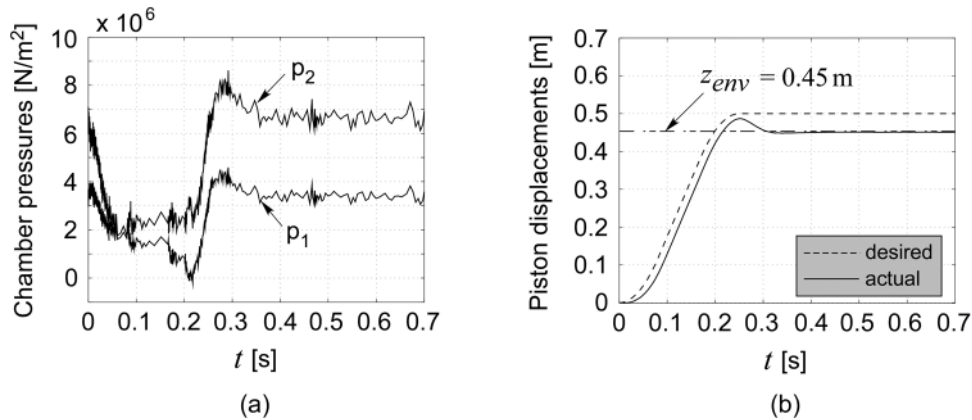
Fig. 13. (a) Chamber pressure sensor histories with experimental noise, and (b) piston displacement responses.

using typical trajectories. The proposed methodology can be extended to electrohydraulic serial or closed-chain manipulators and simulators.

Acknowledgments

References

1. Anderson W. *Controlling Electrohydraulic Systems*. Marcel Dekker Inc., 1988
2. Bilodeau G, Papadopoulos E. A model-based impedance control scheme for high-performance hydraulic joints. In Proceedings of the 1998 International Conference on Intelligent Robots and Systems (IROS '98), Victoria, BC, Canada, October 1998
3. Blackburn JF, Reethof G, Shearer JL. *Fluid Power Control*. MIT Press, Cambridge, MA, 1960
4. Davliakos I, Chatzakos P, Papadopoulos E. Development of a model-based impedance controller for electrohydraulic servos. In Proceedings of the International Conference on Robotics and Applications, Cambridge, MA, 31 October to 2 November 2005
5. Davliakos I, Zafiris A, Papadopoulos E. Joint space controller design for electrohydraulic servos. In Proceedings of the 2006 IEEE International Symposium on Computer-Aided Control Systems Design, (CACSD '06), Tech. Universität München, Munich, Germany, 4–6 October 2006, pp. 796–801
6. Fasse ED, Gosselin CM. Spatio-geometric impedance control of Gough-Stewart platforms. *IEEE Trans Robot Autom* 1999; 15(2): 281–288
7. Gao XS, Lei D, Liao Q, Zhang GF. Generalized Stewart-Gough platforms and their direct kinematics. *IEEE Trans Robot* 2005; 21(2): 141–151
8. Garagic D, Srinivasan K. Application of nonlinear adaptive control techniques to an electrohydraulic velocity servomechanism. *IEEE Trans Control Syst Technol* 2004; 12(2): 303–314
9. Gough VE. Discussion in London: automobile stability, control, and tyre performance. In Proceedings of the IMechE's Automobile Division, 1956, pp. 392–394
10. Ha QP, Nguyen QH, Rye DC, Durrant-Whyte HF. Impedance control of a hydraulically actuated robotic excavator. *Autom Constr* 2000; 9: 421–435
11. Heinrichs B, Sepehri N, Thornton-Trump AB. Position-based impedance control of an industrial hydraulic manipulator. *IEEE Control Syst* 1997; 46–52
12. Helouvry BA, Dupont P, De Wit CC. A survey of models, analysis tools and compensation methods for the control of machines with friction. *Automatica* 1994; 30(7): 1083–1138
13. Hogan N. Impedance control: an approach to manipulation: part I – theory, part II – implementation, part III – applications. *ASME J Dyn Syst Meas Control* 1985; 107: 1–24
14. Jelali M, Kroll A. *Hydraulic Servosystems: Modelling, Identification and Control*. Springer, 2003
15. Lebret G, Liu K, Lewis FL. Dynamic analysis and control of a Stewart platform manipulator. *J Robot Syst* 1993; 10(5): 629–655
16. Liu MJ, Li CX, Li CN. Generalized Stewart-Gough platforms and their direct kinematics. *IEEE Trans Robot Autom* 2000; 16(1): 94–98
17. Merritt HE. *Hydraulic Control Systems*. John Wiley, 1967
18. Niksefat N, Sepehri N. Robust force controller design for an electro-hydraulic actuator based on nonlinear model. In Proceedings of the 1999 IEEE International Conference Robotics & Automation, San Francisco, 1999, pp. 200–206
19. Rosenberg R, Karnopp D. *Introduction to Physical System Dynamics*. McGraw Hill, New York, 1983
20. Rowell D, Wormley DN. *System Dynamics: An Introduction*, Prentice Hall, 1997
21. The True Origins of Parallel Robots, http://www.parallemic.org
22. Sadjadian H, Taghirad HD. Impedance control of the hydraulic shoulder: a 3-DOF parallel manipulator. In Impedance Control of the 2006 IEEE International

Conference on Robotics and Biomimetics, Kunming, China, 2006, pp. 526–531

23. Sirouspour MR, Salcudean SE. Nonlinear control of hydraulic robots. *IEEE Trans Robot Autom* 2001; 17(2): 173–182

24. Stewart D. A platform with six degrees of freedom. In Proceedings of the IMechE, Vol. 180, Pt. 1, No. 15, 1965–1966, pp. 371–385

25. Tafazoli S, Salcudean SE, Zaad KH, Lawrence PD. Impedance control of a teleoperated excavator. *IEEE Trans Control Syst Tech* 2002; 10(3): 355–367

26. Thayer WJ. Specification standards for electrohydraulic flow control servovalves. Technical Bulletin 117, Moog Incorporation Control Division, East Aurora, New York, 1962

27. Tsai LW. *Robot Analysis: The Mechanics of Serial and Parallel Manipulators*. John Wiley & Sons, 1999

28. Tsai LW. Solving the inverse dynamics of a Stewart-Gough manipulator by the principle of virtual work. *Trans ASME, J Mech Des* 2000; 122: 3–9

Appendix A

The 6×6 overall Jacobian matrix, $\mathbf{J}(\mathbf{x})$, combines the generalized velocities, $\dot{\mathbf{x}}$, with the actuator velocities, $\dot{\ell} = \left(\dot{\ell}_1, \dot{\ell}_2, \ldots, \dot{\ell}_6 \right)^{\mathrm{T}}$ via the relationship [27],

$$\dot{\ell} = \mathbf{J}(\mathbf{x}) \cdot \dot{\mathbf{x}} \tag{A1}$$

This equation leads to,

$$\dot{\mathbf{x}} = [\mathbf{J}(\mathbf{x})]^{-1} \cdot \dot{\ell} \tag{A2a}$$

$$\ddot{\mathbf{x}} = [\mathbf{J}(\mathbf{x})]^{-1} \cdot \ddot{\ell} - [\mathbf{J}(\mathbf{x})]^{-1} \dot{\mathbf{J}}(\mathbf{x}, \dot{\mathbf{x}}) \cdot \dot{\mathbf{x}} \tag{A2b}$$

Finally, substitution of Eq. (A2b) in Eq. (1), yields Eq. (4).

Appendix B

In this Appendix, the proof for Eq. (16) is outlined.

The pressure drops of the servovalve orifice 1 and 2, see Fig. 3b, are given by,

$$\Delta P_{G_1}(i) = C_{G_1}^{-1} \cdot Q_{v1} |Q_{v1}| \tag{B1a}$$

$$\Delta P_{G_2}(i) = C_{G_2}^{-1} \cdot Q_{v2} |Q_{v2}| \tag{B1b}$$

The flow Q_{v1} is found using the flow continuity law, along with servovalve input, i.e.,

$$Q_{v1}(i) = Q_{I,\ell1} - Q_{v2}(i) \tag{B2}$$

Substituting Eq. (B2) in (B1a), is following results,

$$\Delta P_{G_1}(i) = C_{G_1}^{-1} \cdot (Q_{I,\ell1} - Q_{v2}) |(Q_{I,\ell1} - Q_{v2})| \tag{B3}$$

Further, the pressure drop of the servovalve orifice 2 is written as,

$$\Delta P_{G_2}(i) = \Delta P_{G_1}(i) + P_1 - P_2 \tag{B4}$$

Taking into account the Eq. (B1b), the last equation is written as,

$$C_{G_2}^{-1} \cdot Q_{v2} |Q_{v2}| = \Delta P_{G_1}(i) + P_1 - P_2 \tag{B5}$$

Eqs. (B3) and (B5) are two nonlinear algebraic equations in the unknowns pressure drop $\Delta P_{G_1}(i)$, and flow Q_{v2}. Solving this system, Eq. (16a) is obtained. Eq. (16b) is obtained similarly.

Appendix C

The actuator lengths are determined using inverse kinematics of the mechanism. Given the generalized coordinates, $\mathbf{x} = (x_0, y_0, z_0, p, q, r)^{\mathrm{T}}$, the actuator lengths are expressed by,

$$
\begin{aligned}
\ell_i = \{ & x_{B_i}^2 + y_{B_i}^2 + z_{B_i}^2 + (X_{A_i} - x_0)^2 + (Y_{A_i} - y_0)^2 \\
& + (Z_{A_i} - z_0)^2 - 2\,[(r_{11}x_{B_i} + r_{12}y_{B_i} + r_{13}z_{B_i}) \\
& \cdot (X_{A_i} - x_0) + (r_{21}x_{B_i} + r_{22}y_{B_i} + r_{23}z_{B_i}) \\
& \cdot (Y_{A_i} - y_0) + (r_{31}x_{B_i} + r_{32}y_{B_i} + r_{33}z_{B_i}) \\
& \cdot (Z_{A_i} - z_0)]\}^{1/2}, \qquad i = 1, 2, \ldots, 6
\end{aligned}
\tag{C1}
$$

where $X_{A_i}, Y_{A_i}, Z_{A_i}$ are the coordinates of joints A_i relative to XYZ frame, see Fig. 8, $x_{B_i}, y_{B_i}, z_{B_i}$ are the coordinates of joints B_i relative to xyz frame, see Fig. 8, and $r_{11}, r_{12}, \ldots, r_{33}$ are the elements of rotation matrix of the platform, which are given by,

$$
\begin{aligned}
r_{11} &= \cos p \cos q \cos r - \sin p \sin r, \\
r_{12} &= -\cos r \sin p - \cos p \cos q \sin r, \\
r_{13} &= \cos p \sin q
\end{aligned}
\tag{C2a}
$$

$$
\begin{aligned}
r_{21} &= \cos q \cos r \sin p + \cos p \sin r, \\
r_{22} &= \cos p \cos r - \cos q \sin p \sin r, \\
r_{23} &= \sin p \sin q
\end{aligned}
\tag{C2b}
$$

$$
\begin{aligned}
r_{31} &= -\cos \gamma \sin q, \quad r_{32} = \sin q \sin r, \\
r_{33} &= \cos q
\end{aligned}
\tag{C2c}
$$

Appendix D

The 6×6 mass matrix of the platform, **M**, and 6×1 vectors **V** and **G** of the Stewart mechanism, in case that the dynamics of mechanism actuators is neglected, are given by,

$$\mathbf{M} = \begin{pmatrix} m & 0 & 0 & 0 & 0 & 0 \\ 0 & m & 0 & 0 & 0 & 0 \\ 0 & 0 & m & 0 & 0 & 0 \\ 0 & 0 & 0 & M(4,4) & M(4,5) & I_{zz}\cos q \\ 0 & 0 & 0 & M(5,4) & M(5,5) & 0 \\ 0 & 0 & 0 & I_{zz}\cos q & 0 & I_{zz} \end{pmatrix}$$

$$\text{(D1a)}$$

$$\mathbf{V} = (0, 0, 0, V(4,1), V(5,1), V(6,1))^{\mathrm{T}}$$

$$\text{(D1b)}$$

$$\mathbf{G} = (0, 0, 0, mg, 0, 0)^{\mathrm{T}} \tag{D1c}$$

where,

$$M(4,5) = M(5,4) = \frac{1}{2}(I_{yy} - I_{xx}) \cdot \sin q \cdot \sin 2r$$

$$\text{(D2a)}$$

$$M(4,4) = \frac{1}{4}[I_{xx} + I_{yy} + 2I_{zz} - (I_{xx} + I_{yy} - 2I_{zz})$$
$$\cdot \cos 2q + 2 \cdot (I_{xx} - I_{yy}) \cdot \cos 2r \cdot \sin^2 q]$$

$$\text{(D2b)}$$

$$M(5,5) = \frac{1}{2}[I_{xx} + I_{yy} + (I_{yy} - I_{xx}) \cdot \sin 2r]$$

$$\text{(D2c)}$$

and,

$$V(4,1) = \frac{1}{2}\Big\{(I_{yy} - I_{xx})\dot{q}^2 \cos q \cdot \sin 2r$$
$$- 2I_{zz}\dot{q}\,\dot{r}\sin q - 2(I_{xx} - I_{yy})$$
$$\cdot \dot{q}\,\dot{r}\sin q \cdot \cos 2r + [I_{xx} + I_{yy} - 2I_{zz}$$
$$+ (I_{xx} - I_{yy})\cos 2r] \cdot \dot{p}\dot{q}\sin 2q$$
$$+ (I_{yy} - I_{xx})\dot{p}\dot{q}\,\dot{r}\sin^2 q \cdot \sin 2r\Big\}$$

$$\text{(D3a)}$$

$$V(5,1) = \frac{1}{4}\Big\{[2I_{zz} - I_{xx} - I_{yy} - (I_{xx} - I_{yy})$$
$$\cos 2r]\dot{p}^2 \cos 2q + 4[I_{zz} + (I_{yy} - I_{xx})$$
$$\cos 2\gamma]\dot{p}\,\dot{r}\sin q + 4(I_{xx} - I_{yy})\dot{q}\,\dot{r}\sin 2r\Big\}$$

$$\text{(D3b)}$$

$$V(6,1) = \frac{1}{2}\Big\{(I_{xx} - I_{yy})\dot{p}^2 \sin^2 q \cdot \sin 2r$$
$$- 2[I_{zz} + (I_{yy} - I_{xx}) \cdot \cos 2r]\dot{p}\,\dot{q}\sin q$$
$$- (I_{xx} - I_{yy})\dot{q}^2 \sin 2r\Big\}$$

$$\text{(D3c)}$$